

The CABRI fast neutrons Hodoscope: CABRI model and signal-to-mass conversion charts

Vincent Chevalier^{1,*} and Jacques Di Salvo¹

¹IRSN, PSN-RES/SEREX/L2EP, Cadarache, F-13108 Saint-Paul-Lez-Durance, France

(*) vincent.chevalier@irsn.fr

Abstract— The CABRI experimental pulse reactor, located at the Cadarache nuclear research center, southern France, is devoted to the study of Reactivity Initiated Accidents (RIA). The hodoscope, installed in the CABRI reactor, is a unique online fuel motion monitoring system, operated by IRSN. This equipment is dedicated to the measurement of the fast neutrons emitted by the tested rod, in real time (with a rate of 1ms), during the power pulse. It is one of the distinctive features of the CABRI reactor facility, which is operated by CEA. To support the experimental task around CABRI reactor, by the experimenters who work on the Hodoscope, a Monte Carlo model, using the MORET code, is used by IRSN. This paper presents the main outcomes obtained during the reactor commissioning tests functioning, using Hodoscope results compared to MORET calculations, which proves the validity of the CABRI MORET model. Furthermore, we show how MORET code is used to build the signal-to-mass conversion charts of the Hodoscope.

Keywords —CABRI, Hodoscope, RIA transient, fast neutron detection system, MORET simulations.

I. INTRODUCTION

FOR enhancing safety of Nuclear Power Plants (NPP), the French Institute for Radiological Protection and Nuclear Safety (IRSN) carries out some experimental programs in order to improve the understanding of the fuel behavior under severe accident conditions. One of them is the CABRI International Program, managed and funded by IRSN under an OECD/NEA agreement. The program is devoted to the study of Reactivity Initiated Accidents (RIA) in representative Pressurized Water Reactor (PWR) conditions [1].

For this purpose, the renovation of the CABRI facility has been conducted by the French Alternative and Atomic Energies (CEA), its operator. This pool type reactor is designed to submit a test rod placed in the center of the core to a RIA. A Pressurized Water Loop, to reproduce the thermal hydraulic conditions of a Pressurized Water Reactor (PWR), for testing the cladding of a fuel rod under prototypical conditions of RIA in PWRs, has been implemented in the center of the core. This so-called test cell is filled with the experimental device during a CABRI transient. It can also receive a system maintaining different dosimeters, with or without water filling the loop during these kinds of experiments.

The CABRI facility is equipped with two nondestructive measurement systems operated by IRSN teams:

- The IRIS facility, for performing X-ray radiography and tomography imaging before and after a power transient thanks to a linear electron accelerator, as well as quantitative gamma scanning analyses [2].
- The Hodoscope, an online fuel motion measurement system, which aims at analyzing the fuel motion deduced from the detection of fast neutrons emitted by the tested rod, in real time (with a time step of 1ms) during the transient [3].

In Section II of this article, a brief description of the hodoscope measuring system will be given. In Section III, comparison between dosimetry and Hodoscope's detectors measurements are shown. Then, section IV, these experimental results will be compared to numerical Monte Carlo simulations. These calculations are thereafter used to build signal-to-mass conversion charts, that are presented in section V. Finally, conclusion and perspectives of work are given.

II. GENERAL DESCRIPTION OF THE SYSTEM

The CABRI reactor has been equipped with the hodoscope since 1977. This system measures in real time the behavior of the test rod in the center of the CABRI core during the transient. The hodoscope is able to quantify the amount of fuel ejected in the milliseconds following failure, time-dependent axial fuel mass distributions and to follow the fuel clusters after failure. In addition, the initial state of the test rod is precisely known thanks to the hodoscope measurement as well as the fissile length and the axial power profile.

The hodoscope centerpiece is a 3 m steel collimator (in green in Fig. 1) of 3 columns and 51 rows, so 153 channels. Behind each one of these line-of-sights, a ²³⁷Np Fission Chamber detector (FC) and a Proton Recoil proportional detector (PR) measure the fast neutrons coming from the core and test rod. Two different technologies of detectors are used in CABRI in order to follow all the experiments from low power (~50 kW) up to 20 GW. Proton recoil counters are better suited for low power (up to ~1 GW which means 2.5 million impulsions per second), thanks to a higher efficiency and no discrimination of the γ noise, and ²³⁷Np fission chambers are used for higher power. They have low gamma sensitivity, and an energy threshold of 650 keV. The signal acquisition rate may be adjusted between 1 ms and 10 s according to the count rate.

The hodoscope collimator has three different degrees of freedom, for adjusting its position in front of the test rod. The distance from the collimator nose to the core axis may be adjusted manually in translation, while two Direct Current Motors are used to move the collimator in verticality and rotation. Each one of the 306 detectors is linked by a μ -metal cable to its electronic chain placed 30 m far from the detector. These electronics have been renewed taking benefit from the renovation period [4].

To keep the signal-to-noise ratio as low as possible [5], the CABRI driver core is traversed radially by the irradiation channel. In that way, none of the fuel rods of the core are in direct view of the hodoscope detectors. Nevertheless, the signal-to-noise ratio remains low and requires specific data treatment algorithms.

The collimator was installed to make a pixelization of the test rod placed in the center of the reactor. Each detector looks at a slice of the test rod. In steady state conditions, the signals measured by all detectors are stable, whereas in transient conditions (i.e. a RIA pulse) they may vary according to a fuel displacement, a fuel densification (yielding to an increasing signal), or a fuel dilution or ejection (yielding to a decreasing signal).

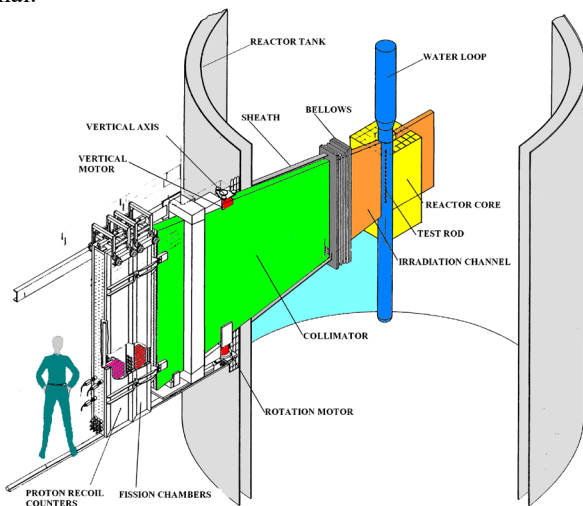


Fig. 1. Hodoscope detector system.

III. HODOSCOPE EXPERIMENTAL RESULTS COMPARED TO DOSIMETRY MEASUREMENTS

The CABRI commissioning campaign included several experiences with dosimetry measurements [6].

Wire dosimeters were placed at several known elevations in the center of the test cell to measure the axial power profile of the CABRI core. Two irradiation campaigns have been performed: one with the test cell in air and one with the test cell filled with water. These results were compared to those obtained with the hodoscope PR detectors, in order to determine their qualitative response. Fig. 2 and Fig. 3 respectively present the axial profile measured with the PR detectors of the hodoscope and the dosimeter counting rates, for water or air filling the loop. The power plateau for these experiences were set at 30 kW (respectively 3 kW).

For this comparison, new sensitivity coefficients, estimated during the calibration campaign of hodoscope detectors, performed in 2018, are used [7].

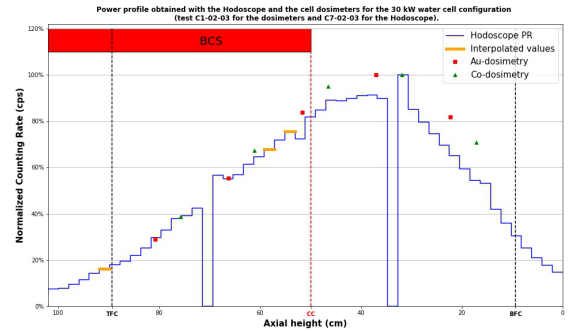


Fig. 2. Comparison between the counting rate measured by the Hodoscope and the “water cell” dosimetry.

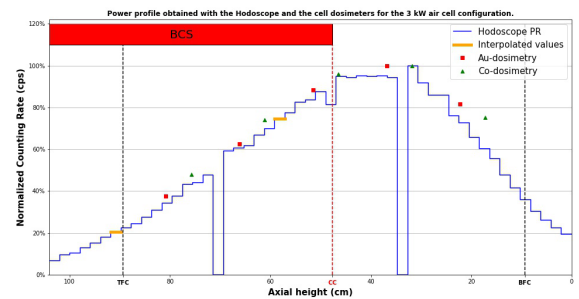


Fig. 3. Comparison between the counting rate measured by the Hodoscope and the “air cell” dosimetry.

An important aspect to observe in these graphs is that hodoscope PR detectors measure fast neutron flux coming from the core, whereas dosimeters measure thermal and epithermal fluxes of the core. Consistency between these curves is due to a constant ratio between thermal and fast flux during steady state conditions. This assumption is also verified in transient conditions.

The position of the Control and Safety Rods (BCS) has been plotted, this allows a better understanding of the profile of the neutron flux.

Indeed, these rods are made of hafnium which is a neutron absorber, the fast neutrons from the fuel rods are therefore less present in the areas of the test cell located at the same height as these rods. This then distorts the theoretical flux shape of the parallelepipedic core, following a "cosine" function. Transient bars filled with helium-3 also play the role of neutron absorber on CABRI in order to quickly reduce the power of the reactor, however in the various tests carried out during these campaigns, these bars did not contain helium-3.

In conclusion, the profile obtained with the new sensitivity coefficients is more suited with the dosimetry measurements, compared to previous results presented in [3].

IV. COMPARISON WITH NUMERICAL SIMULATION

In order to solve the Boltzmann Equation, for CABRI reactor, Monte Carlo MORET code [8], developed by IRSN, has been used to determine some neutronic parameters.

In this section, results obtained with MORET 5C, using JEFF3.1.1 library [9], are compared to experimental results. Monte Carlo codes give results in steady state conditions. The MORET model of the CABRI core is shown on Fig. 4.

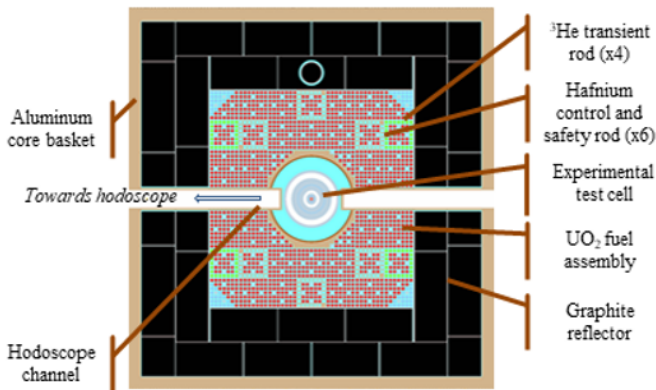


Fig. 4. MORET Model of the CABRI core.

A. MORET calculation compared to hodoscope results

A comparison has been carried out with hodoscope experimental results obtained during a 23 MW power plateau. In order to present these results, the same 2018 sensitivity coefficients have been applied to the Hodoscope measurements. The MORET simulation was made by representing a lead rod inside the experimental device, in the center of the test cell. This dummy rod has been cut into cylinders of 2cm-high (representing the projections of the Hodoscope channels on the test rod).

In this configuration, the BCS are less inserted into the core, because the reactor power being higher (23 MW against a few tens of kW previously). At higher power level, the fuel is hotter, leading to a broadening of the resonances and therefore of the increase of core anti-reactivity. The critical position of the control rods obtained is then greater than the previous one. This can also be seen in the shape of the curves, which is much more symmetrical than those at low power (figures in the previous section).

Considering the 2 curves on Fig. 5, a difference at the extremities can however be noticed: the calculations seem to underestimate the flux in these places. This can be partly explained statistically because the neutron flux being lower, the uncertainty on the associated values is higher.

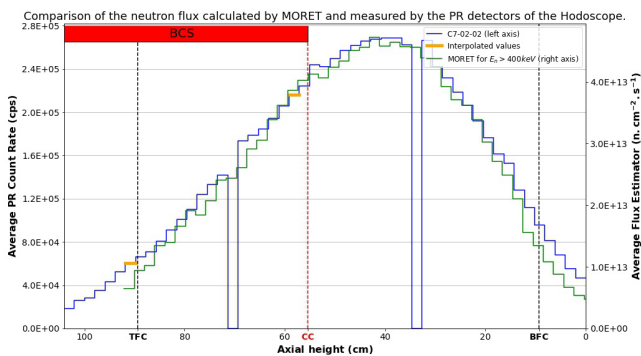


Fig. 5. MORET 5 compared to PR profile steady-state conditions.

B. MORET calculation compared to dosimetry experiments

Another step in the validation of our model consists in simulating the operation of the dosimeters within our modeling. This simulation requires adding several elements within the CABRI core. The experimental conditions of the test corresponding to “air cell” dosimetry, and it was necessary to precisely know the geometry of the dosimeters used and their locations.

10 wired dosimeters were used, including 5 in gold (Au197) and 5 in cobalt (Co59). These wires are extremely thin, 5 mm long and 0.1 mm in diameter (gold) to 0.25 mm in diameter (cobalt).



Fig. 6. Example of dosimeter under quartz (wire made of iron).

They were therefore deposited in quartz capsules 1 mm in radius and about 1 cm in height (Fig. 6). These 10 dosimeters were then placed in an aluminum dosimeter holder tube according to the following diagram (Fig. 7).

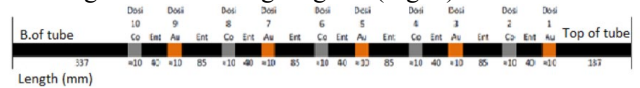


Fig. 7. Dosimeter's layout diagrams.

This 6 mm diameter of the holder tube replaces the entire test device in the center of the cell and is fixed by two aluminum centralizers located at its ends.

A MORET model was therefore carried out by reproducing the following various elements as exactly as possible: the tube, the centering devices, the quartz capsules, and the gold and cobalt wires. After configuring the different chemical compositions of the elements used, reaction rates (n, γ) were requested as output for each volume of gold and cobalt wires. As the volume of the wire is tiny, the reaction rate is low, and the uncertainties remain therefore substantial (between 10% and 15%). However, it can be notice in the following Figures, that the relative profiles calculated by the MORET code are in good agreement with cobalt dosimeter measurements and show some limited differences with gold dosimeter measurements.

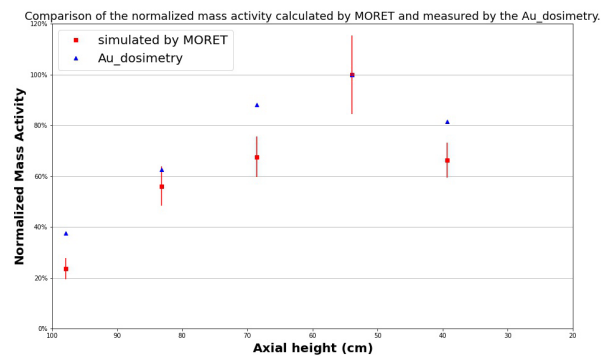


Fig. 8. Comparison between measured and computed specific activities of “cell air” for dosimeters in gold.

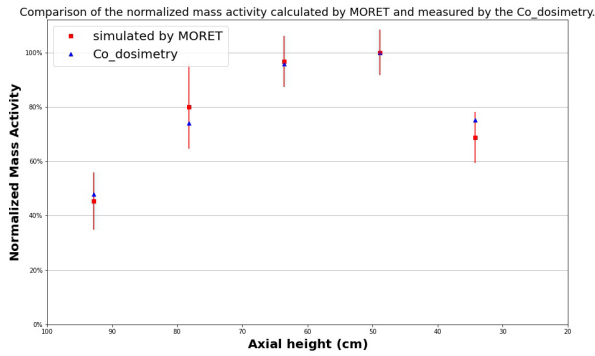


Fig. 9. Comparison between measured and computed specific activities of “cell air” for dosimeters in cobalt.

Despite these relative differences, we can consider a rather good ability of our CABRI model with MORET, to account for physical reality regarding flux variations. Moreover, this model is used for relative calculations, as it will be explained in the next section.

V. SIGNAL-TO-MASS CONVERSION CHARTS

A. Axial distribution signal

Thanks to the Hodoscope software it’s possible to obtain the axial distribution of the signals recorded by FC during a test. This is one of the most important hodoscope measurements, performed during the transient. The axial distribution is made up of the ratio of the “useful signal” (neutrons coming from the rod, in the line of sight of the corresponding row, monitored for each of the Hodoscope line) to the “noise” (neutrons from the core) measured by the detectors over time ($SNR(t)$), divided by the value of this same ratio recorded during the power plateau, before the transient, (SNR_0).

The experimentalist then evaluates, on this axial distribution, the different periods of time where a fuel motion seems to have been occurred. This is evidenced by the value of the aforementioned report. Indeed, if $SNR(t)/SNR_0 > 1$, this means an increase of the mass of fuel on the line and during the time interval considered. Conversely, if $SNR(t)/SNR_0 < 1$, this reflects a mass deficit.

As an example, from a real test, the $SNR(t)/SNR_0$ ratio, displayed in Fig. 10 for the hodoscope rows 19 to 25, describes fuel motions during a power transient. For a given row, a ratio greater (respectively lower) than one is represented in green (respectively red) on the Fig. 10.

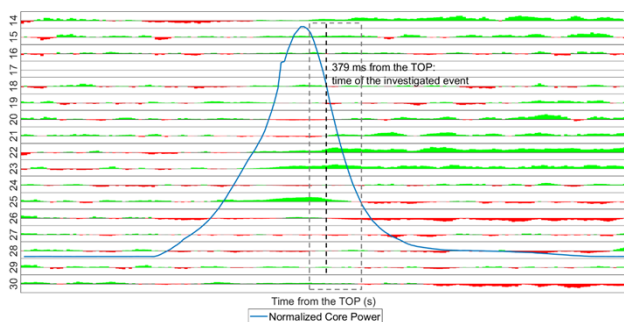


Fig. 10. Axial distribution.

The grey dashed rectangle (around $T0+379$ ms) delimits the time interval where a significant fuel motion started: a fuel accumulation for the rows 22 and 23, followed later by a lack of fuel for the rows 25 to 30.

B. Signal-to-mass conversion charts

In order to be able to quantify these mass movements highlighted by the axial distribution signal, the experimentalist uses the signal/mass conversion charts.

The value of $SNR(t)/SNR_0$ is linked to the ratio of fission rate of the test rod during the transient, to the fission rate of this same intact rod (before the transient) [10].

These fissions rates are computed for different ideal degradation configurations that the rod could have during the transient, as well as for the intact rod configuration, to obtain the normalized ratio of fission rates. These calculations are realized using the CABRI model, performed with the IRSN MORET code, for a given critical state configuration. It is important to note that this normalized ratio ($\Sigma\Phi/\Sigma_0\Phi$) is independent of the axial profile.

To build signal/mass conversion charts, 6 configurations of the test rod were imagined in addition to that corresponding to the intact test rod. By noting m_0 the fissile mass of the initial fuel in the rod section considered and m , the fissile mass of the fuel in the considered configuration, we can characterize these different models by the ratio m/m_0 .

It is important to note that even if these configurations are ideal, they could represent a real case. Anyway, they are to be considered as points of reference to build the charts. They are presented on the Fig. 11.

Conf.	Mass ratio	Conf.	Mass ratio
	Fuel intact $\frac{m}{m_0} = 1$		Intact pellet, fuel relocated between the cladding rod and the test device channel $\frac{m}{m_0} = 1.5$ (change of the density)
	Fuel motion outside the cladding rod $\frac{m}{m_0} = 1$ (change of the density)		Fuel ejected from the cladding rod, presence of relocated fuel between the cladding and the test device channel $\frac{m}{m_0} = 1.5$ (change of the density)
	Hole in the center of fuel $\frac{m}{m_0} = 0.7$		Complete obstruction of the channel by relocated fuel $\frac{m}{m_0} = max$
	Fuel motion outside the cladding rod $\frac{m}{m_0} = 0.7$ (change of the density)		

Fig. 11. The seven ideal configurations.

The charts resulting from the 7 MORET calculations on these configurations are plotted in the Fig. 12.

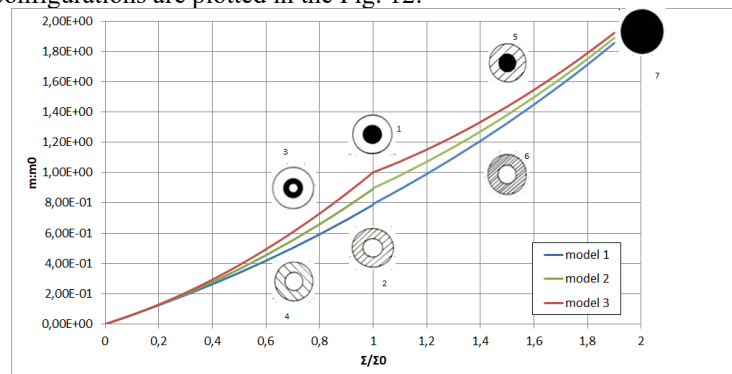


Fig. 12. Signal-to-mass conversion charts.

The different configurations are:

- Configuration 1 is the reference, the m/m_0 ratio is 1 and all the fuel is inside the cladding.
- Configurations 2, 4 and 6 correspond to a situation where the fuel has left the clad and is located between it and the channel test device (corresponding to the so-called “model 1” in the Fig. 12. They respectively have a ratio $m/m_0 = 1, 0.7$ and 1.5 .
- Configuration 3 corresponds to core meltdown, i.e., the fuel is located inside the clad but the central part has been destroyed, giving a ratio $m/m_0 = 0.7$.
- In configuration 5, the fuel pellet is still intact, but additional fuel coming from upstream has been added, between the clad and the channel test device with a ratio $m/m_0 = 1.5$. The three cases 1,3,5 constitute the so-called “model3” in the Fig. 12.
- For the last configuration, case 7, the inner section of the channel test device is completely filled with fuel, which gives $m/m_0 = 3.5$.

The “model 2” is made up by taking the intermediate cases between those of “model 1” and those of “model 3”.

To carry out these seven simulations, the experimentalist must know the isotopic composition of the rod as well as that of its cladding, then modify the mass concentrations of the constituent elements of the fuel scattered around the cladding (for cases 2, 4, 5 and 6).

The MORET model can take into account the influence of the spatial self-shielding effect by modeling 3 slices of axial degradation of the test rod.

C. Application to a real case

The axial distribution signal illustrated in Fig. 10 is first transformed to a signal histogram, by averaging the values in the time period mentioned above, for each slice of the test rod (Fig. 13). One can notice the line without counting rate, which is full of stainless steel in order to assure the mechanical support of the collimator. Then, the signal-to-mass conversion charts is applied to transform the signal histogram to mass histogram (Fig. 14).

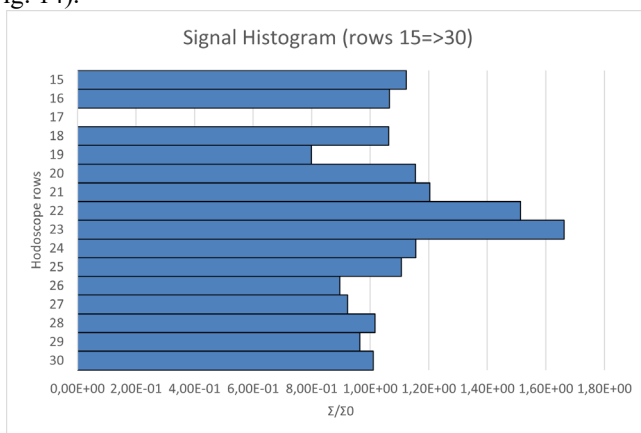


Fig. 13. Signal histogram.

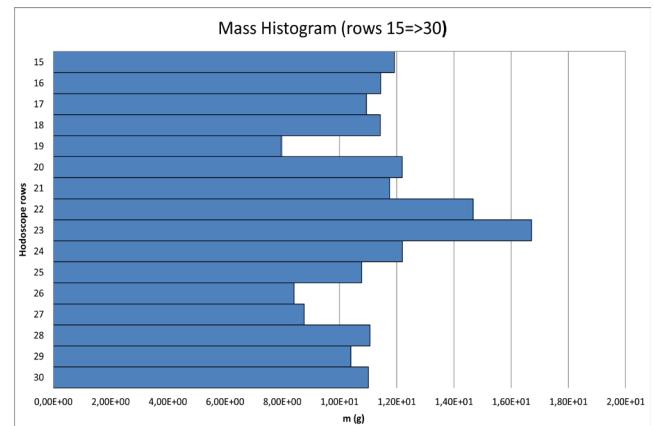


Fig. 14. Mass histogram.

Reproducing this methodology for each time period, it is possible to obtain the fissile mass motion during the whole transient. Hence, to completely analyze the degradation of a test rod, it is required to create a suited scenario, combining all the events spotted in the axial distribution to the corresponding degradation configurations.

VI. CONCLUSIONS AND PERSPECTIVES

This paper presents the experimental validation of a MORET model, which is used to analyze the hodoscope measurements monitored during a reactivity transient in the CABRI reactor.

The MORET model has been compared to results coming from the hodoscope calibration campaign, as well as from a dedicated neutron activation dosimetry characterization.

The neutron flux profile, calculated by MORET at the center of the CABRI reactor, is consistent with the hodoscope detectors measurements. For the comparison to the specific activities of the gold and cobalt dosimeters, the MORET calculations show some limited differences to the measurements, despite high calculations uncertainties. As this model is used for fission rates ratio calculations, this validation has been considered sufficiently satisfying.

Different configurations, considering different degradations of the test rod, have then been simulated with the model, in order to obtain signal-to-mass conversion charts. Thanks to these charts, the quantitative mass motion of the test rod can be directly deduced from signal histograms, acquired by hodoscope detectors all along the transient, and requiring the creation of a scenario of degradation.

The definition of this scenario is a manual combination of the choice of the degradation models, for each line of the hodoscope. Further developments could be studied, to automate this combination. Besides, a complementary work of the estimation of the resolution of the Hodoscope, has been undertaken, in order to be able to use it in the case of fuel relocation during or after the test

ACKNOWLEDGMENT

The authors thanks J. Andries, who made its internship in the laboratory, for its contribution to this work.

REFERENCES

- [1] B. Biard et al, "Reactivity Initiated Accident transient testing on irradiated fuel rods in PWR conditions: The CABRI International Program," *Annals of Nuclear Energy*, Vol **141**, 15 June 2020, 10.1016/j.anucene.2019.107253.
- [2] Q. Grando et al, "CABRI test events monitoring through three measurement systems," in *Proc. ANIMMA, Prague, Czech Republic, 2021. EPJ Web of Conferences*, Vol **253**, 04013 (2021), 10.1051/epjconf/202125304013.
- [3] V. Chevalier et al, "The CABRI fast neutron Hodoscope: Renovation, qualification program and first results following the experimental reactor restart," in *Proc. ANIMMA, Liège, Belgium, 2017. EPJ Web of Conferences*, Vol **170**, 04003 (2018), 10.1051/epjconf/201817004003.
- [4] S. Mirotta et al, "Qualification and characterization of electronics of the fast neutron Hodoscope detectors using neutrons from CABRI core," in *Proc. ANIMMA, Liège, Belgium, 2017. EPJ Web of Conferences*, Vol **170**, 04016 (2018), 10.1051/epjconf/201817004016.
- [5] J. Di Salvo et al, "Signal-to-Noise Ratio of CABRI hodoscope: Monte Carlo calculation versus experiments," *IEEE Trans. On Nuclear Science*, Vol **69**, n°4, pp. 648-655, April 2022, 10.1109/TNS.2022.3150069.
- [6] J. Lecerf et al, "Analysis of the dosimetry campaign performed during the CABRI commissioning tests," in *Proc. ANIMMA, Liège, Belgium, 2017. hal-02418142*.
- [7] V. Chevalier et al, "The CABRI fast neutron Hodoscope: calibration campaign results," in *Proc. RRFM, Helsinki, Finland, 2020. hal-03080772*.
- [8] B. Cochet et al, "Capabilities overview of the MORET5 Monte Carlo code," *Annals of Nuclear Energy*, Vol **82**, pp. 74-84, August 2015, 10.1016/j.anucene.2014.08.022.
- [9] A. Santamarina et al, "The JEFF-3.1.1 Nuclear Data Library. Validation results from JEF2-2 to JEFF-3.1.1.," *JEFF Report 22*, ISBN 978-92-64-99074-6. © OECD 2009.
- [10] K. Baumung et al, "Quantitative fuel motion determination with the CABRI fast neutron hodoscope: Evaluation methods and results," *Nucl. Technology*, Vol **96**, pp. 302-311, June 1991.